Charge transfer and ionization in collisions of Si^{3+} with H from low to high energy

J. G. Wang, B. He, Y. Ning, C. L. Liu, and J. Yan
Key Laboratory of Computational Physics, Institute of Applied Physics and Computational Mathematics, Beijing 100088, China

P. C. Stancil
Department of Physics and Astronomy and the Center for Simulational Physics, University of Georgia, Athens, Georgia 30602-2451, USA

D. R. Schultz
Physics Division, Oak Ridge National Laboratory, Oak Ridge, Tennessee 37831-6373, USA
(Received 28 August 2006; published 15 November 2006)

Charge transfer processes due to collisions of ground state $Si^{3+}(3s\ ^1S)$ ions with atomic hydrogen are investigated using the quantum-mechanical molecular-orbital close-coupling (MOCC) and classical-trajectory Monte Carlo (CTMC) methods. The MOCC calculations utilize *ab initio* adiabatic potentials and nonadiabatic radial coupling matrix elements obtained from Herrero *et al.* [J. Phys. B **29**, 5583 (1996)] which were calculated with a full configuration-interaction method. Total and state-selective single-electron capture cross sections are obtained for collision energies from 0.01 eV/u to 1 MeV/u. Total and state-selective rate coefficients are also presented for temperatures from 2×10^3 K to 10^7 K. Comparison with existing data reveals that the total CTMC cross sections are in good agreement with the experimental measurements at the higher considered energies and that previous Landau-Zener calculations underestimate the total rate coefficients by a factor of up to two. The CTMC calculations of target ionization are presented for high energies.

DOI: 10.1103/PhysRevA.74.052709 PACS number(s): 34.50.−s, 34.10.+x

I. INTRODUCTION

Charge transfer in collisions of highly charged ions with neutral atoms and molecules has attracted much attention. This interest stems not only from fundamental aspects but also from the importance of electron capture processes in astrophysics and plasma physics. Charge transfer provides a recombination mechanism for multiply charged ions in x-ray ionized astronomical environments which may have sparse electron abundances [1]. In the divertor region of a tokamak fusion device, charge exchange of impurity ions with neutral atoms and molecules plays an important role in the ionization balance and the production of radiative energy loss leading to cooling [2,3]. In the core of the plasma, charge exchange spectra produced by neutral beam injection is also an important method to diagnose the populations of impurities. Recently, it has been found that ion-atom/molecule charge transfer processes are of particular significance to EUV and x-ray emission from comets and from planetary atmospheres. Soft x-ray emission has been observed from many comets including comet Hale-Bopp [4] and comet Hyakutake [5,6]. It has been suggested that the x-ray emission is due to charge transfer of heavy solar wind ions [such as O^{q+}, C^{q+}, Ne^{q+}, and Si^{q+} $(q=3-8)$] with cometary neutral species such as H, O, H_2, H_2O, OH, and CO [7,8]. Indeed, analysis of x-ray and EUV spectra of comet Hyakutake [9] is said to have confirmed that such charge transfer processes are responsible for the observed x-ray emission. In a similar way, x-ray emission from the Jovian aurora are thought to be driven by charge transfer in collisions of multiply charged oxygen and sulfur ions with atmospheric neutrals such as H, He, and H_2 [10,11]. In inertial confinement fusion (ICF) research, recent experiments suggests that charge transfer may be needed to explain some unusual high-intensity silicon spectra in the high-density and high-temperature plasma [12,13]. In order to model and understand the behavior of these environments, it is necessary to obtain total and state-selective capture cross sections.

In the present paper, the charge transfer process

$$Si^{3+}(3s) + H(1s) \rightarrow Si^{2+}(3s^2,3s3p,3p^2,3s3d,3snl;n \geq 4) + H^+ \quad (1)$$

is studied using the quantum-mechanical MOCC and CTMC methods. Kim *et al.* [14] measured the total single-electron capture cross sections for high collision energies from 50 to 200 keV/u. Butler and Dalgarno [15] estimated the rate coefficients for temperatures between 10^3 K to $10^{4.5}$ K using the Landau-Zener method with empirical parameters. Recently, Herrero *et al.* [16] carried out molecular structure calculations and also estimated total cross sections and rate coefficients using the Landau-Zener method with *ab initio* parameters. The current MOCC calculations utilize *ab initio* adiabatic potentials and nonadiabatic radial coupling matrix elements obtained from the work of Herrero *et al.* who used a full configuration-interaction method. In the current manuscript, total and state-selective cross sections and rate coefficients are obtained and compared with experimental results and other calculations.

II. THEORETICAL METHODS

In the present work, the MOCC and CTMC methods are utilized to calculate total and state-selective charge-transfer cross sections and rate coefficients.

A. MOCC method

The MOCC method, which we only briefly discuss here, has been described thoroughly in the literature (e.g., Kimura and Lane [17], Zygelman *et al.* [18], Wang *et al.* [19]). It involves solving a coupled set of second-order differential equations using the logarithmic-derivative method of Johnson [20]. In the adiabatic representation, transitions between channels are driven by radial and rotational elements of the vector potential $A(\vec{R})$, where $\vec{R}$ is the internuclear distance vector. Since the adiabatic description contains first-order derivatives, it is numerically convenient to make a unitary transformation [18,21,22], which is affected by the radial portion of $A(\vec{R})$, to a diabatic representation

$$U(R) = W(R)[V(R) - P(R)]W^{-1}(R), \tag{2}$$

where $U(R)$ is the diabatic potential matrix, $V(R)$ is the diagonal adiabatic potential, $W(R)$ is a unitary transformation matrix, and $P(R)$ is the rotational matrix of the vector potential $A(\vec{R})$ [19,23,24]. With the diabatic potentials and couplings, the coupled set of second-order differential equations is solved to obtain the K matrix from the scattering amplitude after a partial-wave decomposition (e.g., Zygelman *et al.* [18]). The electron capture cross section is then given by

$$\sigma_{i\to j} = \frac{\pi}{k_i^2}\sum_J (2J+1)|S_J|_{i,j}^2, \tag{3}$$

where the S matrix is

$$\underline{S}_J = [\underline{I} + i\underline{K}_J]^{-1}[\underline{I} - i\underline{K}_J] \tag{4}$$

and $\underline{I}$ is the identity matrix. In this work, the electron translation factors (ETFs; e.g., [17]), which are often used to modify the molecular eigenfunctions to remove asymptotic couplings between atomic states that are connected by dipole transitions, are not included. The influence of ETFs is expected to be important for $E > 1-5$ keV/u (e.g., [25,26]), which is close to the maximum calculated energy of this work.

B. The CTMC method

The CTMC method simulates an ion-atom collision by sampling trajectories computed from a large ensemble of initial projectile-target configurations (e.g., Abrines and Percival [27,28]). In the calculations, the collisions are considered as a three-body problem, that is, the incident Si^{3+} ion, target proton, and the electron initially bound to the target. The initial electronic orbits on the target are prepared in such a way as to mimic the quantum mechanical distributions. The motion of the particles is then determined by an iterative solution of Hamilton's equations of motion. At the end of each Monte Carlo trajectory, the relative classical binding energies are calculated to determine if a reaction (charge transfer, ionization, elastic scattering, etc.) occurred. The final n,l state after target excitation or charge transfer to the projectile can be determined assuming the Bohr model and making a classical-quantum correspondence following the binning rules of Becker and MacKellar [29]. However, as in previous work considering charge transfer in $S^{4+}+H$ [30] and $S^{4+}+He$ [31], we find that the determination of the final projectile state for partially stripped ions, especially for low-lying n levels, using the Becker and MacKellar binning does not always lead to reasonable results since it is only applicable to purely hydrogenic systems or to Rydberg states. Schultz *et al.* [32] and Rakovic *et al.* [33] suggested modifications by incorporating a binning-energy-dependent effective charge or through a quantum defect, respectively. In the present paper, the modification through a quantum defect is utilized with the quantum defect calculated by a multiconfiguration Hartree-Fock method with relativistic corrections [34].

For partially stripped ion impact on H, the interaction of the ion with the electron initially resident on H is represented by a model potential that in effect varies the screening experienced by the electron as it approaches the incident nucleus [35], which is expressed by the formula

$$V(r) = \frac{1}{r}\left(Z - (N-1)\left[1 - \frac{1}{(\eta/\xi)(e^{\xi r}-1)+1}\right]\right), \tag{5}$$

where Z and N are the nuclear charge and number of electrons including the captured electron, and η and ξ are parameters to be determined by fitting the numerical potential. This formula satisfies the asymptotic boundary conditions of the Coulomb potential at small and large electron-incident-ion distances. For Si^{3+} impact on H, the parameters $\eta=3.6638$ and $\xi=2.1824$ are obtained by fitting to the Eq. (5) [35]. If the target is a multielectronic atom or molecule, similar screening model potentials can be applied to the interaction between the electrons and target ions.

III. RESULTS AND DISCUSSIONS

The present MOCC calculations only consider radial couplings and neglect rotational couplings. Since the symmetries of the entrance channels of $Si^{3+}(3s\ ^2S)+H(1s,\ ^2S)$ are singlet sigma ($^1\Sigma^+$) and triplet sigma ($^3\Sigma^+$), we only treat $^{1,3}\Sigma^+$ in the exit channels. In the concerned energy range (0.01 eV/u-10^4 eV/u), the exoergic channels are most important for charge transfer processes so that there are four channels in $^1\Sigma^+$ included in the MOCC calculations, that is, $Si^{2+}(3s^2\ ^1S)+H^+(1\ ^1\Sigma^+)$, $Si^{2+}(3s3p\ ^1P^o)+H^+(2\ ^1\Sigma^+)$, $Si^{2+}(3p^2\ ^1D)+H^+(3\ ^1\Sigma^+)$, and $Si^{3+}(3s\ ^2S)+H(1s,^2S)(4\ ^1\Sigma^+)$; there are two channels in $^3\Sigma^+$, $Si^{2+}(3s3p\ ^3P^o)+H^+(1\ ^3\Sigma^+)$, and $Si^{3+}(3s\ ^2S)+H(1s,\ ^2S)(2\ ^3\Sigma^+)$. For the intermediate and high energy range (10^3 eV/u-10^6 eV/u), the CTMC method is utilized to obtain the total and state-selective $(n,l-)$ cross sections including both of the exoergic and endoergic channels. Besides charge transfer, collisional ionization, and excitation are also included in the CTMC calculations.

A. Diabatic potentials and couplings

The energies for the lowest $12\ ^1\Sigma^+$, $8\ ^1\Pi$, $10\ ^3\Sigma^+$, and $8\ ^3\Pi$ molecular states were computed in Ref. [16]. For the

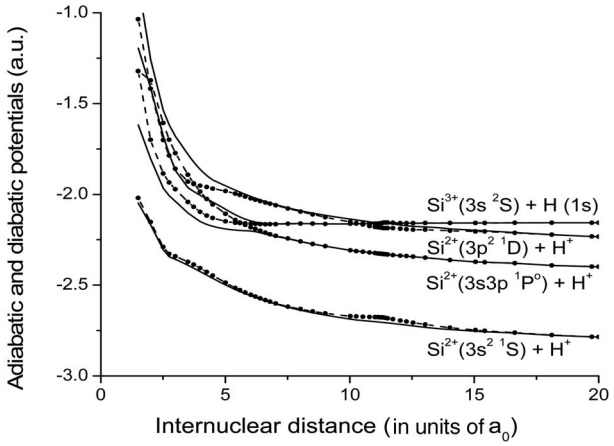

FIG. 1. Adiabatic and diabatic potentials of $[SiH]^{3+}$ ($^1\Sigma^+$) as a function of internuclear distance. Solid lines: adiabatic potentials [16]; Dashed lines with filled circles: diabatic potentials.

four $^1\Sigma^+$ channels and two $^3\Sigma^+$ channels included in the MOCC calculations, comparison with the experimental separated-atom energies [36] shows the absolute errors in these channels are less than 0.272 eV, while the error relative to the entrance channel is less than 0.2 eV, which is adequate for most scattering calculations [16]. Using Eq. (2), the adiabatic potentials and couplings are transformed to the diabatic representation [21,22].

Figure 1 displays the adiabatic and diabatic potentials of $[SiH]^{3+}$ ($^1\Sigma^+$) as a function of internuclear distance. There are two avoided crossings between the 3 $^1\Sigma^+$ and 4 $^1\Sigma^+$ channels, an outer one at $R=11.29\ a_0$ and an inner one at $R=4.5\ a_0$; there is one avoided crossing between the 2 $^1\Sigma^+$ and 3 $^1\Sigma^+$ channels at $R\approx 6.1\ a_0$ [16]. A weak avoided crossing exists between the 1 $^1\Sigma^+$ and 2 $^1\Sigma^+$. It is generally the case that intermediate avoided-crossing distances ($\sim$5 to $\sim$14 a_0) are favorable for charge transfer. Furthermore, the longer avoided-crossing distances are advantageous to electron capture in the low collision energy range, while shorter avoided-crossing distances are favorable at higher energies. It can be expected that capture to the 3 $^1\Sigma^+$ channel will dominate at low energies while capture to the 2 $^1\Sigma^+$ will be become important with increasing collision energy.

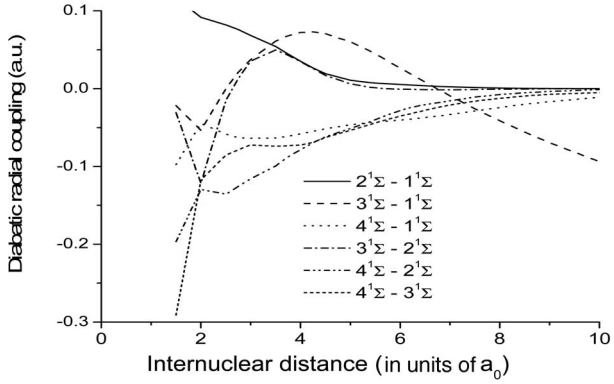

FIG. 2. Diabatic radial couplings of $[SiH]^{3+}$ ($^1\Sigma^+$) as a function of internuclear distance.

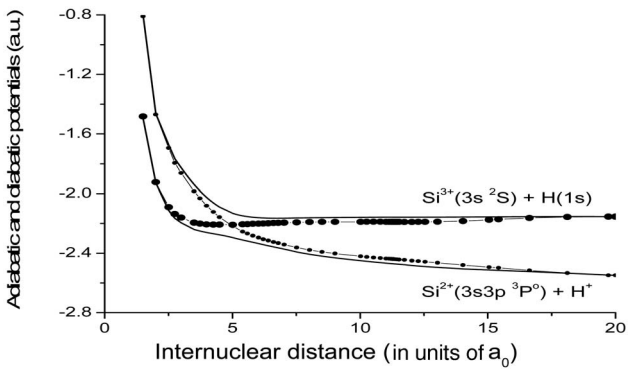

FIG. 3. Adiabatic and diabatic potentials of $[SiH]^{3+}$ ($^3\Sigma^+$) as a function of internuclear distance. Solid lines: adiabatic potentials [16]; Dashed lines with filled circles: diabatic potentials.

Figure 2 plots the diabatic radial couplings of $[SiH]^{3+}$ ($^1\Sigma^+$) as a function of internuclear distance. Except for short internuclear distances ($R<2\ a_0$), the couplings vary smoothly with R. Approaching the united-atom limit, additional avoided crossings may be present which can result in irregular behavior.

The Adiabatic and diabatic potentials of $[SiH]^{3+}$ ($^3\Sigma^+$) are shown in Fig. 3. There is one avoided crossing at $R\approx 5\ a_0$. With this short avoided-crossing distance, the cross section is expected to be small at low energies. The diabatic radial coupling for the ($^3\Sigma^+$) states is plotted in Fig. 4.

B. Total and state-selective cross sections

Using the MOCC and CTMC methods, total and state-selective single-electron capture cross sections for collisions of Si^{3+} with H are calculated from 0.01 eV/u to 1 MeV/u. The total cross sections are displayed in Fig. 5. At the lower collision energies ($E<1$ eV/u), the main mechanism is due to the polarization interaction and the cross section displays the typical Langevin $E^{-1/2}$ behavior. At a collision energy of $\sim$10 eV/u, the total cross section reaches a local minimum, and then increases slowly until the calculated highest energy of 10^4 eV/u is reached. In the MOCC calculations, rotational coupling and endoergic channels are neglected, so that the cross sections at the higher energies, $E>5$ keV/u, are more

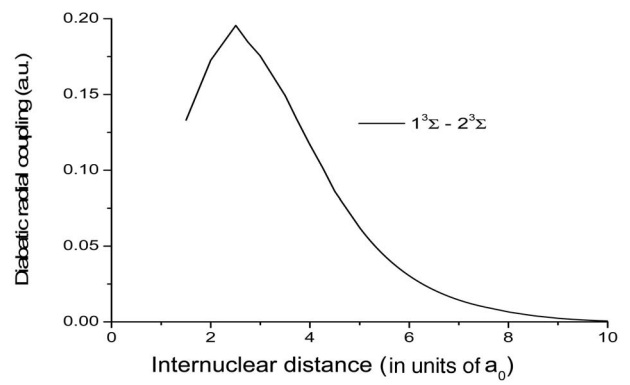

FIG. 4. Diabatic radial couplings of $[SiH]^{3+}$ ($^3\Sigma^+$) as a function of internuclear distance.

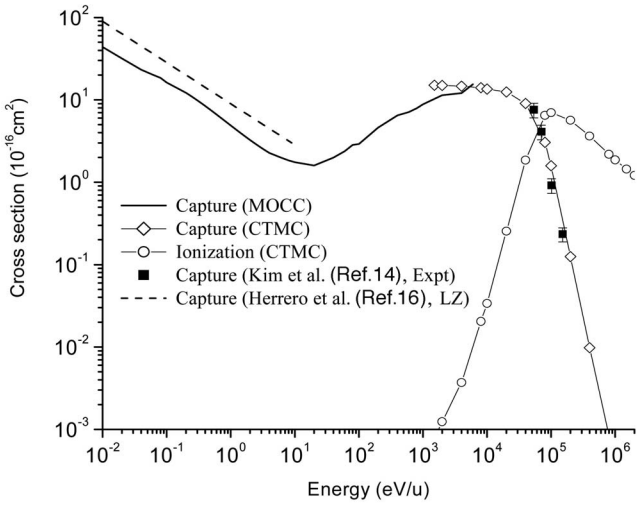

FIG. 5. Total single-electron capture and ionization cross sections for $Si^{3+}+H$. Solid line: present MOCC results for charge transfer; thin solid line with unfilled diamonds: the present CTMC results for charge transfer; thin solid line with unfilled circles: the present CTMC results for ionization; filled squares: experiment [14]; dashed line: Landau-Zener results [16].

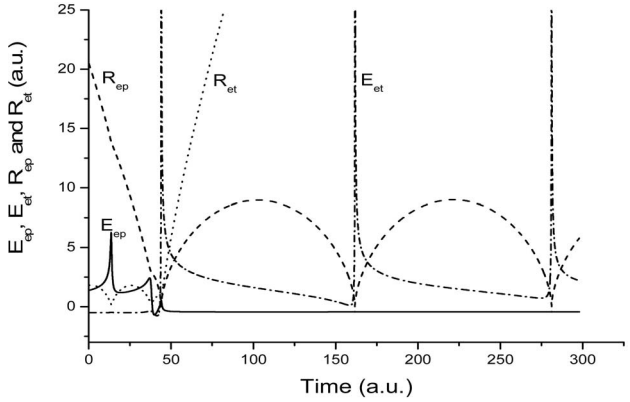

FIG. 6. A classical trajectory at collision energy $E=80$ keV/u as a function of time. Impact parameter $b=9$. Solid line: electron energy relative to the projectile ion; dashed and dotted line: electron energy relative to the target ion; dashed line: distance between electron and the projectile ion; dotted line: distance between electron and target ion.

uncertain [19,30,31]. Herrero *et al.* estimated the total cross section using the Landau-Zener method with *ab initio* parameters and obtained the relation $\sigma=9\times10^{-16}(\mathrm{cm}^2)/\sqrt{E/(\mathrm{eV/u})}$ for the low energy range [16] as plotted in Fig. 5. Comparison with the current MOCC results shows that the Landau-Zener calculations overestimate the cross section by about 60% for $E<1$ eV/u. The relation of Herrero *et al.* is not valid for higher energies.

The CTMC calculations were performed for the higher energy range, $10^3<E<10^6$ eV/u, as shown in Fig. 5. A typical cross section plateau is obtained for energies between 10^3 eV/u and 6×10^4 eV/u, while for $E>6\times10^4$ eV/u, the total cross section drops quickly. In the overlapping energy range of the two calculations, the CTMC results are larger than MOCC calculations, though the MOCC cross sections approach the CTMC results gradually as the collision energy increases from 10^3 eV/u to 10^4 eV/u. In the energy region in which the MOCC and CTMC calculations overlap, they agree well, but the CTMC appears to continue rising at low energies in contradiction to the MOCC. By taking the MOCC cross section at low energies and smoothly joining it to the CTMC result at about 5000 eV, a good estimate of the cross section over the entire energy range of 0.01 eV/u to 10^6 eV/u is obtained.

Kim *et al.* [14] measured the total cross section in the high energy regime as shown in Fig. 5. The CTMC results are in good agreement with the measurements. The collisional ionization cross section calculated with the CTMC method are also presented in Fig. 5. For collision energies less than 10^4 eV/u, the ionization process can be neglected, which justifies the approach in the MOCC method. As the collision energy increases, the ionization cross section increases rapidly. For $E>2\times10^5$ eV/u, the ionization cross section is larger than that of charge transfer. The CTMC calculations include the competition of the various inelastic channels: charge transfer, ionization, and excitation. Another advantage of the CTMC method is that it can give an intuitive physical picture. As an example, we plot one classical trajectory for $E=8\times10^4$ eV/u in Fig. 6. The trajectory shows that the single electron capture process evolves with time. Initially, the electron is far from the incident ion and the electron energy E_{ep}, relative to incident ion, is approximately 1.6 a.u. corresponding to the velocity of incident ion. The electron energy E_{et}, relative to the target ion, remains negative while the distance between the electron and target ion displays an oscillating behavior. As time evolves, the electron moves away from and back toward to the target ion which corresponds to the peaks and troughs for time $t<50$ a.u. For $t>50$ a.u., the distance R_{ep} between the electron and the projectile ion shows an oscillating behavior, and E_{ep} maintains a constant negative value indicating that the electron is captured from the target to the incident ion.

The state-selective single-electron capture cross sections are shown in Fig. 7. In the lower energy region ($E<10$ eV/u), the capture to the $Si^{2+}(3p^2\ ^1D)$ dominates the charge transfer process. This is consistent with the Landau-Zener calculations [15,16] and is a consequence of the avoided crossing at 11.29 a_0 between the entrance channel $Si^{3+}(3s\ ^1S)$ and exit channel $Si^{2+}(3p^2\ ^1D)$, as shown in Fig. 1. It should be noted that $Si^{2+}(3p^2\ ^1D)$ is a doubly excited state so that its formation involves both excitation and capture. With increasing energy, the cross sections for capture to the $3s3p\ ^1P^o$ and $^3P^o$ increase rapidly since there exists avoided crossings at 6.1 a_0 and 5 a_0 for the $^1P^o$ and $^3P^o$, respectively. For $E>30$ eV/u, capture to the $Si^{2+}(3s3p\ ^1P^o)$ becomes the main charge transfer channel. Since the interaction near the avoided crossing for the $Si^{2+}(3s^2\ ^1S)$ channel is weak, the cross section to this channel is small, as shown in Fig. 7(a).

In Fig. 7(b), the so-called triplet-singlet cross section ratio for the $3s3p$, i.e., $^3P^o/^1P^o$, is plotted as a function of collision energy. As has been pointed out in numerous studies where spin-multiplicity can be resolved [19,24,37,38], this ratio deviates significantly from the statistical 3:1 ratio at low

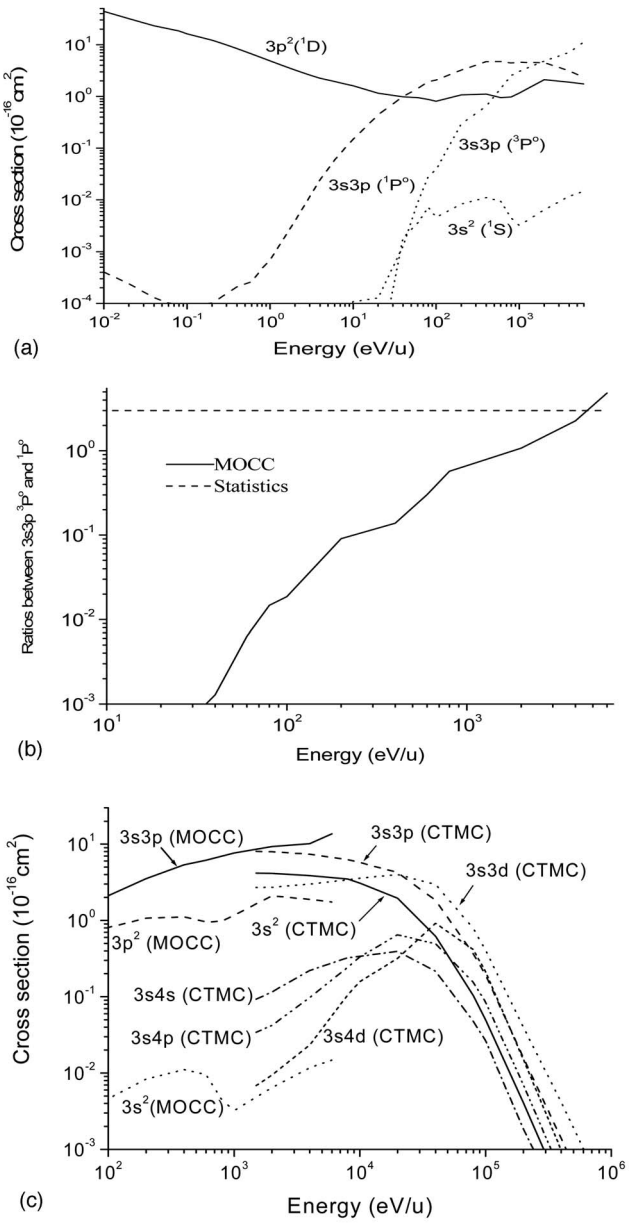

FIG. 7. State-selective single-electron capture cross sections. (a) The MOCC calculations in the collisional energy region $0.01\ \mathrm{eV/u} < E < 5\ \mathrm{keV/u}$. (b) The MOCC results for the $3s3p$ triplet-singlet cross section ratio. (c) The MOCC and CTMC calculations in the energy region $100\ \mathrm{eV/u} < E < 1000\ \mathrm{keV/u}$.

energy. The statistical ratio is only recovered at the highest energies considered in the MOCC calculations.

The state-selective CTMC cross sections are plotted in Fig. 7(c) which only includes the one-electron processes (i.e., the doubly excited state $Si^{2+}(3p^2)$ is not considered) since the present CTMC model treats only one active electron moving in the screened Coulomb field of the target nucleus. The importance of capture into $Si^{2+}(3snl)$ is dependent on both the binding energies of the final states and the incident energies of the ion. For $10^3 < E < 10^4$ eV/u, except $Si^{2+}(3s^2)$, the cross sections vary from largest to smallest in the order from high to low final state binding energy of

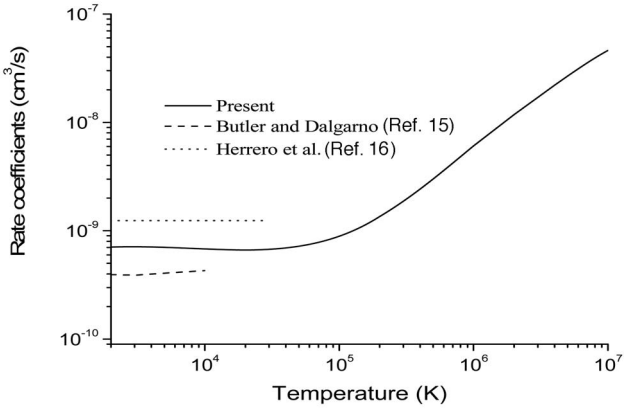

FIG. 8. Total rate coefficients in charge transfer of $Si^{3+}(3s\ ^2S)$ with H as a function of temperature. Solid line: present results; dashed line: Butler and Dalgarno [15]; dotted line: Herrero *et al.* [16].

$Si^{2+}(3snl)$, that is, from $Si^{2+}(3s3p)$ to $Si^{2+}(3s4d)$. Similar to the MOCC results, the cross section for capture to $Si^{2+}(3s^2)$ is much smaller than that for capture to $Si^{2+}(3s3p)$ and $Si^{2+}(3s3d)$, although electron capture to $Si^{2+}(3s^2)$ is also an exoergic process. With increasing incident energy, the importance of electron capture to the higher l excited states increases, so that the cross section for capture to $Si^{2+}(3s4d)$ is larger than $Si^{2+}(3s4p)$ and $Si^{2+}(3s4s)$ and the cross section for capture to $Si^{2+}(3s3d)$ is larger than $Si^{2+}(3s3p)$ and $Si^{2+}(3s^2)$ when $E > 10^5$ eV/u.

Compared to the MOCC calculations, the CTMC results in the overlapping energy range are too large for capture to the $Si^{2+}(3s^2\ ^1S)$ state, owing most likely to the single-electron treatment implicit in the present CTMC approach. Again, we note that by about 1–5 keV/u the general lower limit of the CTMC's applicability for charge transfer is being reached and the need for a true two-electron approach to describe the state-selective results is likely as well. On the other hand, the cross sections for capture to the $Si^{2+}(3s3p)$ show good agreement between the two methods. The $Si^{2+}(3s3d)$ and higher excited states are not included in the MOCC calculations. If the $Si^{2+}(3s3d)$ and $Si^{2+}(3s4s)$ were included in the MOCC calculations, but their cross section would be expected to decrease with decreasing energy unlike the CTMC behavior which may partially explain the discrepancy in the total cross sections seen in Fig. 5.

C. Total and state-selective rate coefficients

Total and state-selective charge transfer rate coefficients were calculated using the cross sections obtained by the MOCC method. Total charge transfer rate coefficients for $Si^{3+}(3s\ ^2S)$ with H are plotted in Fig. 8. For lower temperatures ($T < 10^5$ K), the total rate coefficients are nearly constant with a value of $7 \times 10^{-10}\ \mathrm{cm^3/s}$. This is a consequence of the low-energy Langevin behavior in the total cross section. But for $T > 10^5$ K, the rate coefficient increases with the increasing temperature. Comparing to other theoretical work, the Landau-Zener calculations with empirical parameters

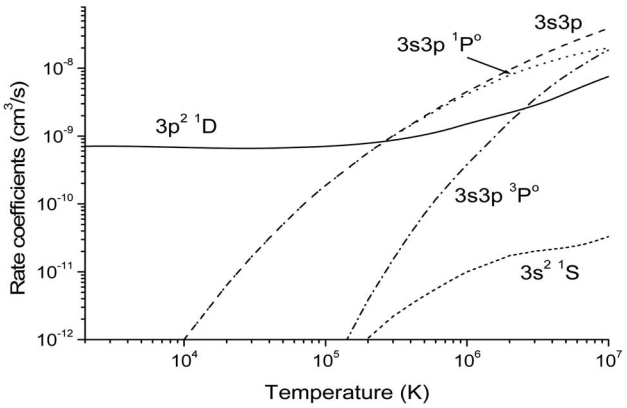

FIG. 9. State-selective rate coefficients in charge transfer of $Si^{3+}(3s\ ^2S)$ with H as a function of temperature.

[15] underestimate the total rate coefficients by a factor of two while the Landau-Zener calculations with *ab initio* parameters [16] overestimate the total rate coefficients by about the same factor. Herrero *et al.* might make a mistyping for the rate coefficient in Ref. [16]. We obtain the rate coefficient of 1.24×10^{-9} cm^3/s from their cross section at energy E of $9\times10^{-16}(\mathrm{cm}^2)/\sqrt{E/(\mathrm{eV/u})}$ [16], which is plotted in Fig. 8.

State-selective rate coefficients in charge transfer of $Si^{3+}(3s\ ^2S)$ with H are plotted in Fig. 9. For the lower temperature range ($T<10^5$ K), the charge transfer process for capture to the $Si^{2+}(3p^2\ ^1D)$ dominates over the other channels and maintains a constant value of about 7×10^{-10} cm^3/s. With increasing temperature, the rate coefficients for capture to the $Si^{2+}(3s3p\ ^{1,3}P^o)$ increase rapidly. For the temperature range 2×10^5 K$<T<10^7$ K, capture to the $Si^{2+}(3s3p\ ^1P^o)$ is the dominant channel. For $T>10^7$ K, capture to $Si^{2+}(3s3p\ ^3P^o)$ becomes the most important channel. The rate coefficients for capture to the $Si^{2+}(3s^2\ ^1S)$ can be neglected for the calculated temperature range. These are in accordance with the state-selective cross sections in Fig. 7(a). The total and state-selective rate coefficients are also tabulated in Table I.

IV. SUMMARY

Charge transfer processes due to collisions of ground state $Si^{3+}(3s\ ^1S)$ ions with atomic hydrogen are investigated using the quantum-mechanical molecular-orbital close-coupling (MOCC) and the classical-trajectory Monte Carlo (CTMC) methods. Total and state-selective single-electron capture cross sections are obtained for collision energies from 0.01 eV/u to 1 MeV/u. Total and state-selective rate coefficients are also calculated for temperatures between 2×10^3 K and 10^7 K. Comparison with existing data suggests that the CTMC cross sections are about 50% larger than available measurements at high energies and that previous Landau-Zener calculations underestimate or overestimate the total rate coefficient by a factor of two. The MOCC method is appropriate to be applied to the low energy, while the CTMC method is appropriate at the higher energies. Further theoretical and experimental studies are needed to validate the current work.

TABLE I. Total and state-selective charge transfer rate coefficients (cm^3/s) as a function of temperature. Numbers in square brackets denote powers of 10.

T (K)	Total	$3p^2\ ^1D$	$3s3p\ ^1P^o$	$3s3p\ ^3P^o$	$3s^2\ ^1S$
2000	7.08 [10]	7.08 [−10]	1.42 [−14]	1.14 [−16]	6.38 [−16]
4000	7.09 [−10]	7.09 [−10]	6.77 [−14]	1.92 [−16]	7.77 [−16]
6000	7.00 [−10]	6.97 [−10]	2.20 [−13]	2.97 [−16]	8.68 [−16]
8000	6.87 [−10]	6.87 [−10]	5.21 [−13]	4.60 [−16]	9.41 [−16]
10000	6.79 [−10]	6.78 [−10]	9.99 [−13]	7.05 [−16]	1.01 [−15]
20000	6.66 [−10]	6.59 [−10]	6.36 [−12]	3.68 [−15]	1.28 [−15]
40000	6.96 [−10]	6.64 [−10]	3.15 [−11]	1.62 [−14]	2.43 [−15]
60000	7.50 [−10]	6.77 [−10]	7.26 [−11]	3.98 [−14]	1.41 [−14]
80000	8.16 [−10]	6.90 [−10]	1.26 [−10]	1.03 [−13]	5.59 [−14]
100000	8.92 [−10]	7.05 [−10]	1.87 [−10]	2.55 [−13]	1.40 [−13]
200000	1.35 [−09]	7.85 [−10]	5.66 [−10]	3.87 [−12]	1.05 [−12]
400000	2.43 [−09]	9.52 [−10]	1.43 [−09]	3.74 [−11]	3.31 [−12]
600000	3.60 [−09]	1.14 [−09]	2.34 [−09]	1.15 [−10]	5.55 [−12]
800000	4.82 [−09]	1.32 [−09]	3.26 [−09]	2.30 [−10]	7.81 [−12]
1000000	6.05 [−09]	1.50 [−09]	4.16 [−09]	3.78 [−10]	9.97 [−12]
2000000	1.18 [−08]	2.21 [−09]	7.94 [−09]	1.63 [−09]	1.73 [−11]
4000000	2.21 [−08]	3.52 [−09]	1.29 [−08]	5.61 [−09]	2.15 [−11]
6000000	3.12 [−08]	4.98 [−09]	1.61 [−08]	1.00 [−08]	2.43 [−11]
8000000	3.92 [−08]	6.37 [−09]	1.84 [−08]	1.45 [−08]	2.84 [−11]
10000000	4.62 [−08]	7.55 [−09]	2.00 [−08]	1.87 [−08]	3.31 [−11]

ACKNOWLEDGMENTS

The authors appreciate helpful discussions with Professor A. S. Dickinson. This work was supported by the National Natural Science Foundation of China (Grant Nos. 10344001, 10574018, and 10574020) and the Science and Technology Foundation of the Chinese Academy of Engineering Physics. J.G.W. and P.C.S. also acknowledge support from the U. S. National Aeronautics and Space Administration through Grant NAG5-11453.

[1] S. Lepp and R. McCray, Astrophys. J. **269**, 560 (1983).
[2] S. I. Krasheninnikov, A. Yu. Pgarov, and D. J. Sigmar, Phys. Lett. A **214**, 295 (1996); **222**, 251 (1996).
[3] R. K. Janev, T. Kato, and J. G. Wang, Phys. Plasmas **7**, 4364 (2000).
[4] A. Owens, A. N. Parmar, T. Oosterbroek *et al.*, Astrophys. J. **493**, L47 (1998).
[5] C. M. Lisse *et al.*, Science **274**, 205 (1996).
[6] M. J. Mumma, V. A. Krasnopolsky, and M. J. Abbott, Astrophys. J. **491**, L125 (1997).
[7] T. E. Cravens, Geophys. Res. Lett. **24**, 105 (1997).
[8] R. M. Haberli, T. I. Gombosi, and D. L. De Zeeuw *et al.*, Science **276**, 939 (1997).
[9] V. A. Krasnopolsky and M. J. Mumma, Astrophys. J. **549**, 629 (2001).
[10] T. E. Cravens, E. Howell, J. H. Waite, Jr., and G. R. Gladstone, J. Geophys. Res., [Atmos.] **100**, 17153 (1995).
[11] W. Liu and D. R. Schultz, Astrophys. J. **530**, 500 (2000).
[12] R. C. Elton *et al.*, J. Quant. Spectrosc. Radiat. Transf. **65**, 185 (2000).
[13] F. B. Rosmej *et al.*, Phys. Rev. E **66**, 056402 (2002).
[14] H. J. Kim, R. A. Phaneuf, F. W. Meyer, and P. H. Stelson, Phys. Rev. A **17**, 854 (1978).
[15] S. E. Butler and A. Dalgarno, Astrophys. J. **241**, 838 (1980).
[16] B. Herrero, I. L. Cooper, and A. S. Dickinson, J. Phys. B **29**, 5583 (1996).
[17] M. Kimura and N. F. Lane, Adv. At., Mol., Opt. Phys. **26**, 79 (1990).
[18] B. Zygelman, D. L. Cooper, M. J. Ford *et al.*, Phys. Rev. A **46**, 3846 (1992).
[19] J. G. Wang *et al.*, Phys. Rev. A **67**, 012710 (2003); **69**, 062703 (2004).
[20] B. R. Johnson, J. Comp. Physiol. **13**, 445 (1973).
[21] T. G. Heil, S. E. Butler, and A. Dalgarno, Phys. Rev. A **27**, 2365 (1983).
[22] D. L. Cooper, N. J. Clarke, P. C. Stancil, and B. Zygelman, Adv. Quantum Chem. **40**, 37 (2001).
[23] B. H. Brandsen and M. R. C. McDowell, *Charge Exchange and the Theory of Ion-Atom Collisions* (Clarendon Press, Oxford, 1992).
[24] A. R. Turner, D. L. Cooper, J. G. Wang, and P. C. Stancil, Phys. Rev. A **68**, 012704 (2003).
[25] R. K. Janev, L. P. Presnyakov, and V. P. Shevelko, *Physics of Highly Charged Ions* (Springer-Verlag, New York, 1985).
[26] L. F. Errea *et al.*, J. Phys. B **27**, 3603 (1994).
[27] R. Abrines and I. C. Percival, Proc. Phys. Soc. London **88**, 861 (1966).
[28] R. E. Olson and A. Salop, Phys. Rev. A **16**, 531 (1977).
[29] R. L. Becker and A. D. MacKellar, J. Phys. B **17**, 3923 (1984).
[30] P. C. Stancil *et al.*, J. Phys. B **34**, 2481 (2001).
[31] J. G. Wang *et al.*, J. Phys. B **35**, 3137 (2002).
[32] D. R. Schultz, P. C. Stancil, and M. J. Rakovic, J. Phys. B **34**, 2739 (2001).
[33] M. J. Rakovic, D. R. Schultz, P. C. Stancil, and R. K. Janev, J. Phys. A **34**, 4753 (2001).
[34] R. D. Cowan, *The Theory of Atomic Structure and Spectra* (University of California Press, Berkeley, CA, 1981).
[35] R. H. Garvey, C. H. Jackman, and A. E. S. Green, Phys. Rev. A **12**, 1144 (1975).
[36] S. Bashkin and J. O. Stoner, *Atomic Energy Levels and Grotrian Diagrams*, Vol. 2 (New York: North-Holland, 1975).
[37] L. F. Errea, L. Mendez, and A. Riera, J. Phys. A **15**, 101 (1982).
[38] V. A. Krasnopolsky, J. B. Greenwood, and P. C. Stancil, Space Sci. Rev. **113**, 271 (2004).